Development of Key Technologies in DPSSL System for Fast-ignition, Laser Fusion Reactor
-FIREX, HALNA, and Protection of Final Optics

T. Norimatsu 1), H. Azechi 1), Y. Fujimoto 1), T. Jitsuno 1), T. Kanabe 1), R. Kodama 1), K. Kondo 1), N. Miyanaga 1), H. Nagatomo 1), M. Nakatsuka 1), H. Shiraga 1), K. A. Tanaka 1), K. Tsubakimoto 1) , M. Yamanaka 1), R. Yasuhara 1), Y. Izawa 1), T. Kawashima 2) , T. Kurita 2), O. Matsumoto 2), Y. Tsuchiya 2), T. Sekine 2), and H. Kan 2)

1)Institute of Laser Engineering, Osaka University, 2-6, Yamada-oka, Suita, Osaka 565-0871, Japan, E-mail; norimats@ile.osaka-u.ac.jp
2)Hamamatsu Photonics K. K., 5000 Hirakuchi, Hamakita, Sizuoka 434-8601, Japan

Abstract. A critical path to a laser fusion power plant is construction of a reliable, efficient, high repetitive energy driver including the relation with the reactor environment. At ILE, Osaka University, FIREX project has been proposed and the phase I to show heating of compressed fuel to 5 keV has started with construction of the FIREX laser. This project will demonstrate physics of fast ignition and elemental studies are carried out to obtain persuasive data to find the path to the goal. A diode-laser-pumped, solid-state-laser (DPSSL) HALNA-10 succeeded in operation of 7.5J output power at 10 Hz rep-rate. Contamination of final optics by metal vapor was studied using a 1/10 model of the beam duct. The result indicated that contamination can be controlled with high speed shutters and a low pressure buffer gas.

1. FIREX laser

In the ILE's strategy of laser development for the FIREX program, the construction of a new peta-watt (PW) laser has two missions, *i.e.*, the technological development of a multi-kJ PW laser and the establishment of amplifier architecture for the FIREX-II laser. The construction of a new PW laser aims at a demonstration of a temperature ≥5 keV in the phase I of FIREX program. The important specifications for the FIREX-I laser which is based on Nd: glass laser are the 10-kJ output energy, the pulse shaping capability (~10 ps trapezoidal pulse) with a rise time ≤2 ps and the high focusability of compressed pulse (≤30 μm spot with encircled energy of better than 50%).[1]

1.1 System overview and layout

The FIREX-I laser system consists of two parts. One is an "amplifier sub-system" which has been installed in a rest area of the laser room and gear room of the GEKKO laser building. And the other part is a "rear end sub-system" including beam transfer optics, pulse compressors and final focusing optics which is now under the construction.

There are many technological issues to be solved to realize required specifications of FIREX-I laser. To deliver the required energy of 10 kJ after the compression, we need an efficient, large-aperture amplifier system and multi-layer dielectric gratings for the pulse compression. A flat-top pulse with a fast rise time is essential for the rapid heating to overcome the expansion loss. Therefore the OPCPA (optical parametric chirped pulse amplification) has been upgraded to ensure a spectral width larger than 3 nm at the output of main amplifier. And the pulse shaping is controlled by adding an appropriate group velocity dispersion depending on the wavelength as an analogy of a Gaussian-to-flat top beam

homogenizer. The beam focusability depends on the tip/tilt-piston error among 4 beams and the wave front aberration within each beam. To minimize the beam-to-beam phase error, the real time phase locking between 4 beams can be feasible using tip/tilt-piston mirrors having a fast response. For the reduction of wave front aberration two or three deformable mirrors will be used in each beam line.

1.2 Present status of FIREX-I laser construction

Figure 1 shows a schematic bird view and key technologies of amplifier. In the multi-pass architecture, the longitudinal focus separation has been adopted in conjunction with the angular multiplexing based on the usual far-field angle separation. The beam is injected into a cavity through an input coupler lens. Here we set this lens at a certain position to give a focal shift of about 1 m that corresponds to 0.5-mrad beam divergence after the collimation by a spatial filter lens. Back-reflected beam goes along another path, and is picked-out from the vacuum. The beam size on the pick-out mirror is adjusted to be almost 10 cm to prevent this mirror from the laser-induced damage. The collimated beam is again reflected back into the cavity along the 3rd path, and finally reflected back toward an output lens of the spatial filter. The size of output beam is $37\times37\text{cm}^2$.

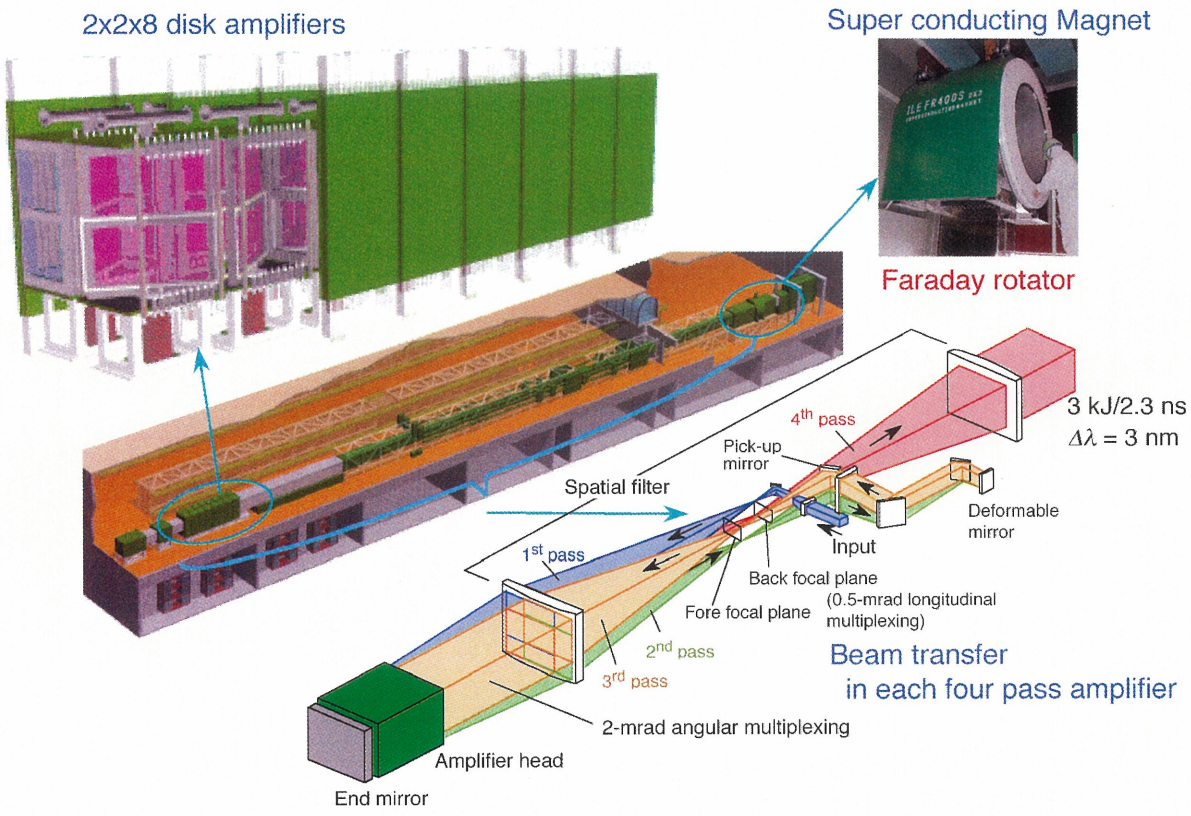

Fig.1 Schematic view and key technologies of amplifier.

The installation of a front end and amplifier system has been completed by the end of March, 2004. This system is now being activated to demonstrate the high-energy chirped pulse amplification. March. The beam transport optics of the rear end sub - system have also been installed, and the rest parts of the rear end will be installed successively by March, 2007.

2. HALNA-DPSSL

In a fast-ignition laser-fusion power-plant, it is required for the laser driver to provide pulse energy of 500 kJ at a repetition rate of 10Hz with 10% overall efficiency. For the demonstration of HALNA (High Average-power Laser for Nuclear-fusion Application) DPSSL (Diode-Pumped Solid-State Laser) driver, we have developed a small test bed of a zig-zag Nd: glass slab DPSSL amplifier [2]. We have attained output energy of 8.5 J per pulse at 0.5 Hz with beam quality of two times diffraction limited (TDL) far-field pattern. For the next step, we have designed new DPSSL system for output energy of 10 J at 10 Hz (HALNA-10).

2.1. System Design

The layout of the laser system is shown in Fig. 2. The laser system incorporated MOPA (Master Oscillator Power Amplifier) configurations. In order to extract energy from a laser medium efficiently, zig-zag slab amplifier through which laser beam passes four times of different optical path in round trip was adopted. A laser oscillator consists of a single longitudinal and transverse mode CW-diode-pumped Nd:YLF seed laser with wavelength of 1053 nm and a diode-pumped Nd:YLF Q-switched slave oscillator. An energy output of the oscillator is 1 mJ. A pre-amplifier is diode-pumped Nd:YLF rod amplifier (LA0318, Hamamatsu Photonics) which amplifies the oscillator output to 300 mJ. The laser beam pattern which passed through a serrated rectangular aperture is transmitted by relay imaging with spatial filters. The high spatial frequency components generated by thermal distortion of the laser glass were removed with pinholes in the spatial filters.

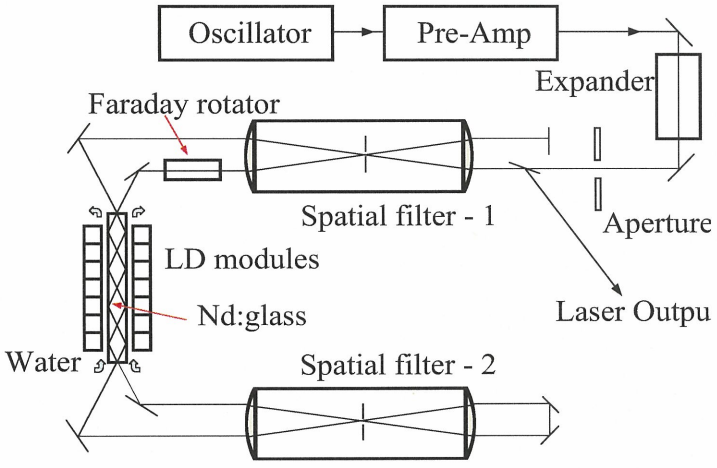

Fig. 2. Schematic diagram of HALNA 10 optical layout,

A laser beam passes through the laser glass of the main amplifier four times in optical zig-zag path. It passes through a Faraday rotator with 45° rotation twice between second path and third path. Passing through the Faraday rotator twice, the final output beam of s- polarization is reflected by a polarizer.

Laser glass geometry was designed in consideration of a damage threshold value, amplification characteristics, and prevention of a parasitic oscillation. The pumping dimension of zig-zag slab glass was decided as 268 mm long, 22 mm high, and 10 mm wide. The entrance and exit faces of the laser glass were coated with sol-gel thin film for anti-

reflection. In order to reduce thermal effect the laser glass was cooled with flowing water through the channel between the laser glass and the window sheet glass. The coolant water flowed with velocity of 1 m/s on the surface of the laser glass.

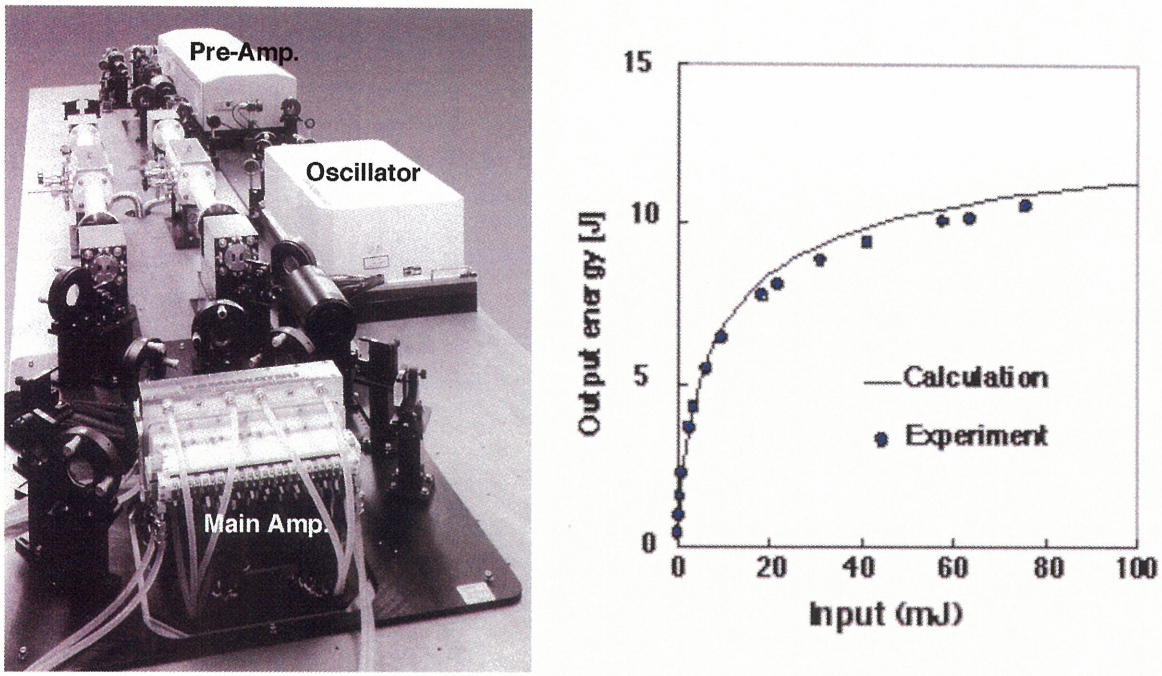

Fig.3. HALNA-10 laser system and calculated results and measured values of 1-Hz operation,

We modified Frantz–Nodvik equation[3] and Eggleston–Frantz equation[4] to derive the equation for laser amplification through a laser medium. The output of 10 J may be obtained from the results of the calculations by pumping energy of 48 J.

A LD stack element was composed of 50 pieces of a quasi-cw, 803-nm, AlGaAs LD bar (Hamamatsu Photonics) with power of 100 W. Spectrum width of 3.4 nm was sufficiently narrow compared to absorption spectrum width of Nd:glass. Cooling water was supplied from the backside of LD bars. Twenty-four stack elements were assembled into a LD module. Total emitting area of the LD module was 268 mm long, 21 mm high, and 10 mm width. The LD module attained to a peak power of 145 kW in 200 μs pulse duration at 10 Hz, and the total electrical to optical conversion efficiency was 53% at 100 A of diode current. Two sets of LD module pumped the laser medium with total energy of 48 J from right and left side. Pump intensity reached 2.5 kW/cm^2. Figure 3(left) shows the total laser system of HALNA-10. Laser performance was examined with this system.

2.2. Experimental

A single-pass small-signal gain (SSG) of 8.5 was achieved with 200 μs pulse duration. The pumping energy was risen up to 52 J. Then it was confirmed that SSG did not depend on repetition rate of pump diodes. In the case of the maximum SSG, a stored energy density of 0.4 J/cm^3 and a pumping efficiency of 45% were obtained. Measured output energy was 10.6 J at 1 Hz and 7.5 J at 10 Hz. The measured values of 1-Hz operation shown in Fig.3(right) are well fitted with calculated results. Comparing with calculated results, laser output energy is small at 10 Hz. It is considered that thermal lensing effect of the laser glass lowered the output energy. The estimated temperature increase was about 40 C° at 10 Hz operation. The extraction efficiency was 43.9% at 1 Hz and 31.1% at 10 Hz. And the optical to optical conversion efficiency was 19.9% at 1 Hz and 14.1% at 10 Hz. A filling factor of 41.5% was achieved by using the serrated aperture to suppress the diffraction. Dissipation of output energy due to thermal lens effect was almost suppressed by uniform pumping of slab. In this result, over an 80% of output energy was focused into five TDL at 10 Hz pumping.

2.3. HALNA Development Plan

The several technological breakthroughs including geometrical optics design and thermal management will allow a 100-W average power (HALNA10: 10 J x 10 Hz) from the HALNA-10 experiment. The next step of a 500-W average power (HALNA50: 50 J x 10 Hz) from two larger slab amplifiers will be performed, and finally a 1-kW average power (HALNA100: 100 J x 10 Hz) from larger slabs will be realized in the near future.

3. Protection of Final Optics

3.1 PROTECTION SCHEME

Our basic scheme to protect the final optics from radiation damages due to high-energy particles from fusion burn is to use a magnetic field for ions and synchronized rotary shutters for neutral metal vapor, and to place the final optics 30m away from the reactor for neutrons. Figure 4 is a conceptual drawing of the beam port. The shutter consists of three disks that synchronously rotate at speeds of ω, ω/4, and ω/16, respectively. An electromagnet is located behind the shutter to kick out energetic ions from the beam port.

The major heat load is mostly that of the alpha particles and ions, because of the short range in the wall material. When the first wall is bombarded with alpha particles, 7-μm-thick liquid LiPb evaporates and expands toward the center of the reactor. Usually the motion of expanding plasma can be described by free-expansion from a high density surface. However, in this case, the velocity of the evaporated vapor is almost constant at approximately 1500 m/s, because the back pressure decreases rapidly due to thermal conduction. As the result, almost 6.6 ms elapses until the blast wave crosses the reactor and reaches the beam port on the opposite side. Since the front of the blast wave is much faster than that of the mass center, the shutter must close within, for example, 2.5 ms (t_s).

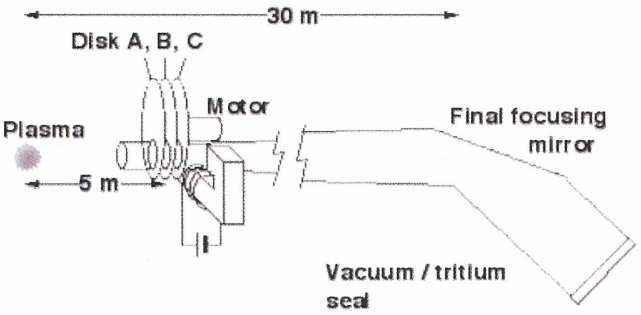

Fig.4 Beam duct and the rotary shutter.

The rotation of disk C must be synchronized with the target irradiation frequency. For example, when the irradiation frequency is 3 Hz, ω must be 96π radian/second. The radii of beams R_b in the fast ignition mode are 0.05 m for compression beams and 0.3 m for the ignition beam. Using the previously determined closing time of 2.5 ms, R_s = 0.93 m for the ignition beam. This size and the rotational speed seem technically acceptable and this scheme of three synchronous rotary shutters will realize a compact mechanical shutter for protection of the final optics.

The rotary shutter blocks the blast wave but the shutter still has an opening time (5 ms) for laser irradiation. Some neutral metal vapor will come into the beam duct and contaminate the final optics. The behavior of the gas may estimated by diffusion model which depends on the radius of molecules. Since we had no date on the diameter of neutral vapor, i. e, single atom molecule or cluster, we studied this issue experimentally and theoretically.

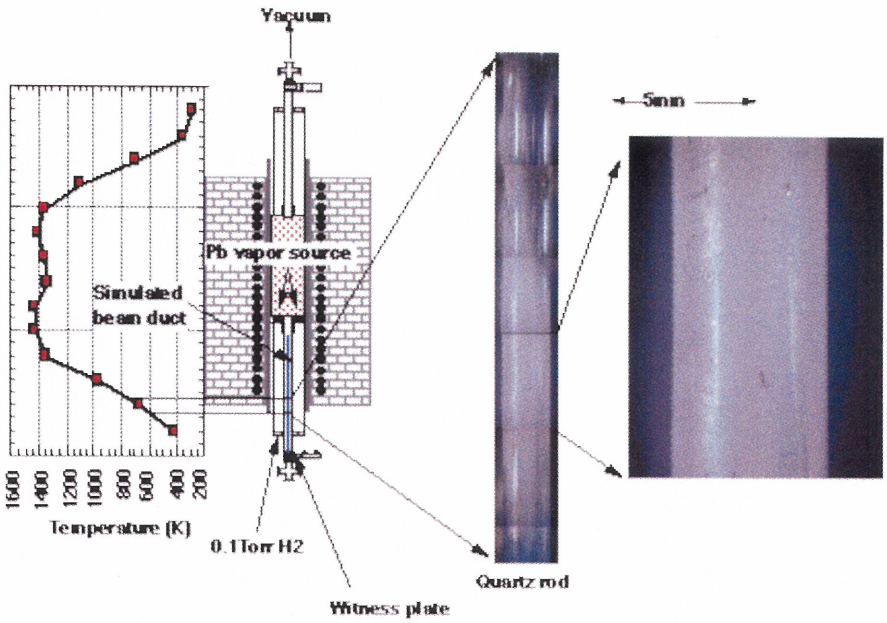

Fig. 5 Experimental setup for simulating diffusion of Pb vapor in a beam duct, and simulation result.

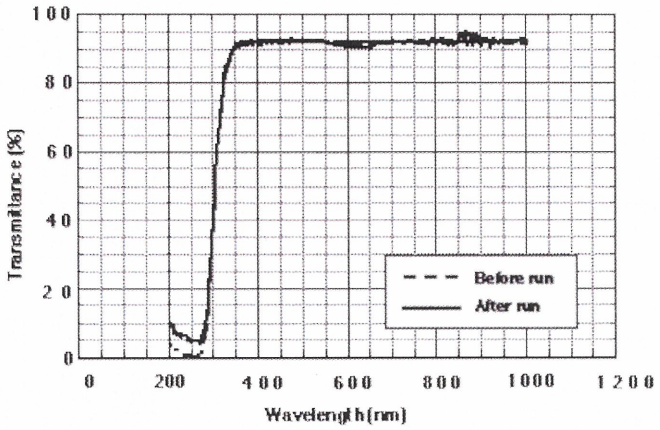

Fig. 6 Transmittance of witness plate

3.2 EXPERIMENTAL

To experimentally simulate contamination of the final optics, a 1/10 scale model of the beam duct was housed in an electric furnace, and 25 g of lead was evaporated at 1400K to provide a Pb vapor pressure of 0.1 Torr. Heating the electric furnace from room temperature to 1400 K took almost 1 hr, and evaporating all the Pb took an additional 40 min. During the operation, the furnace was filled with 0.1 Torr hydrogen, which is representative of DT fuel and the target debris.

In this experiment, Pb was used instead of LiPb. As shown in Fig. 5, a witness plate (final optics) was set at the bottom end of the model duct, where the temperature is 300K, and a 5-mm-diameter, 450 mm long quartz rod was inserted into the duct in order to monitor the deposition of Pb.

As shown in the photographs in Fig. 5, when the back pressure of hydrogen was 0.1 Torr, deposition of Pb on the rod was observed only in a temperature range from 600 K to 800 K. Figure 6 shows transmittance of visible light through the witness plate (1.2 mm thick Pyrex glass) before and after the run. No increase in absorption is observed.

When the back pressure of hydrogen was 10 Torr, numerous small particles (0.1 to $2x10^{-6}$ m in diameter) were deposited on the witness plate; however, no contamination was observed when the back pressure of hydrogen was 0.1 Torr. At 10 Torr, metal vapor seems to be sufficiently cooled in gas phase to form aerosols that deposit on the witness plate. At 0.1 Torr, longer mean free path of the vapor allows quick condensation on the inner surface of the beam duct, but the mean free path is still too short for the metal to contaminate the witness plate on the end of the beam duct. This result indicates that shielding gas can prevent contamination of the final optics in a future laser fusion reactor by thermal metal vapor.

3.3. DISCUSSION

Deposition of Pb was observed only within the temperature range of 600K to 800K. We believe that this can be explained by re-evaporation of Pb. After all the Pb was evaporated, the furnace was maintained at 0.1 Torr during cooling down. Figure 7 shows numerically calculated distribution of Pb atoms in the model duct. In this figure, distance = 0 cm corresponds to the entrance of the beam duct where the vapor pressure of Pb is 0.1 Torr. The duct is filled with 0.1 Torr hydrogen. Number densities of Pb vapor in cells on the duct surface are assumed to be given by that of the saturated vapor pressure of Pb of which temperature is given in Fig. 7. All vapors radially diffusing into the cells are assumed to deposit on the surface. The calculation indicates that the total flow rate of Pb vapor into the duct by diffusion is 2 g/hr.

The calculated result shows that the density of Pb atoms in the duct is mostly determined by the saturated vapor pressure on the duct surface, and this explains why no deposition of Pb was observed on the witness plate located at the distance = -50 cm in this figure.

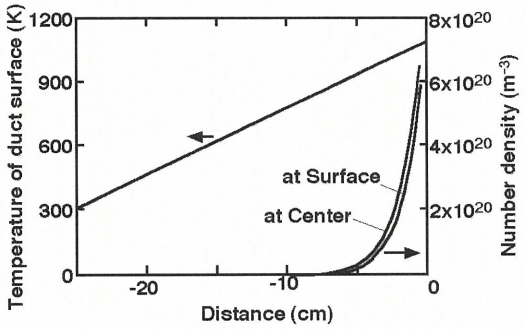

Fig. 7 Distribution of Pb vapor in the duct

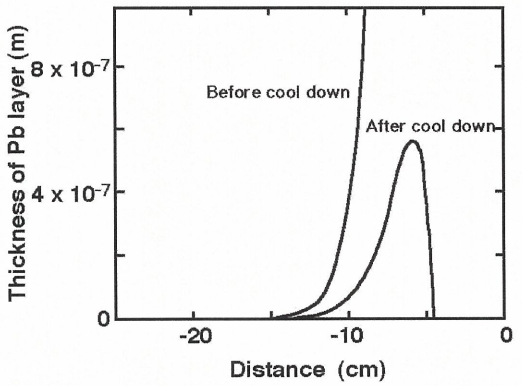

Fig. 8 Thickness of Pb layer after cooling.

Figure 8 shows thickness of the Pb layer on the inner surface of the model duct after cooling. The electric furnace was assumed to have been cooled linearly in two hours after all the Pb was evaporated and the vapor pressure in the furnace became zero. The liquid Pb on the inner surface of the duct is re-evaporated at its theoretical saturated evaporation–rate,

Since the absolute value of Pb thickness strongly depends on the cooling history, comparing this result with experimental results is not completely valid. (In our experiment, Pb deposited on an area between -20 cm and -15 cm. With slower cooling rate, the peak position moves left in this graph.) We can say, however, that Pb in a hot area can re-evaporate during cooling of the furnace.

In a future laser fusion reactor, a radial vapor flow develops under the cryogenic pumping effect of a liquid wall when laser beams irradiate the next target. The velocity of vapor is estimated to be 100 m/s at the inlet of the beam port.[5] The vapor passes through the shutter window and moves in the duct toward the final optics. Figure 9(left) shows temporal change of density, as calculated in consideration of only transverse diffusion. The longitudinal diffusion was ignored for simplification. The temperature of the beam duct is 300 K. Calculation result shows that the density at the duct center decreases to nearly zero in 200 ms.

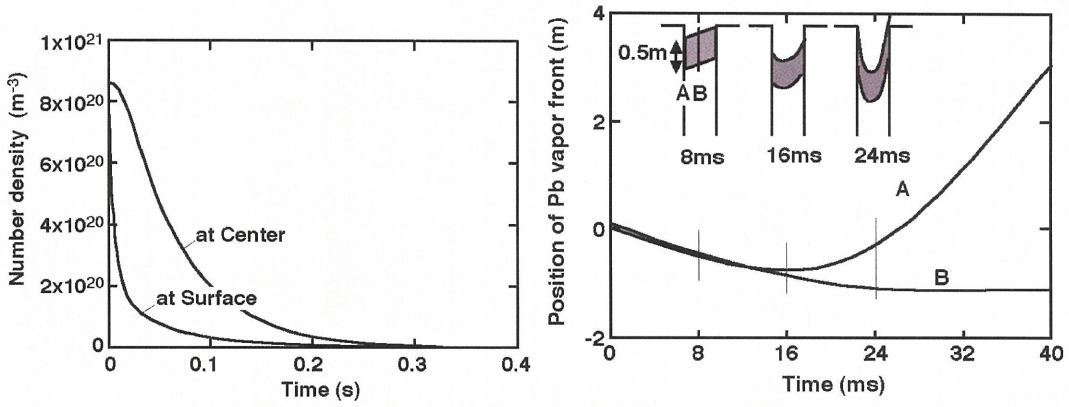

Fig. 9 Number density of Pb vapor calculated from only transversal diffusion (left). Motion of Pb vapor in duct filled with 0.1 Torr hydrogen.(right)

When Pb vapor enters the duct, hydrogen gas in the duct is compressed and the Pb vapor (the total mass 0.4 mg) is decelerated in accordance with its local mass. Numerical analysis of hydrodynamic instabilities with a diffusion process is quite difficult. For simplification, we calculated equation of motions of cells whose masses vary with time as shown in Fig. 9(left).

The result is illustrated in Fig. 9(right). Since spatial thickness of the Pb vapor cloud is 0.5 m, the Pb vapor would break up at about 20 ms. At that time, the velocity of Pb vapor will have decreased to 30 m/s. When we remember that the diffusion process is dominant and the density of Pb vapor decreases in 30 ms, we can see that the Pb vapor front moves only 0.9 m after the break and cannot reach the final optics.

References

[1] MIYANAGA. N., et al., "FIREX petawatt laser development for fast ignition research at ILE, Osaka", Inertial Fusion Sciences and Applications 2003, American Nuclear Society (2004) 507-511.
[2] KAWASHIMA . T., et al. , Jpn. J. Appl. Phys. 40 (2001) 6415-6525.
[3] Frantz . L.M. and Nodvik .J.S., J. Appl. Phys. 34 (1963) 2346-2349.
[4] Eggleston . J.M., Frantz . L.M. and Injeyan . H., IEEE J.Quantum Electron. 25 (1989) 1855-1862.
[5] KOZAKI . Y. et al., presented at 18th IAEA Fusion Energy Conference Sorrento, Italy, 4 to 10 October 2000, IAEA-CN-77/FTP1/27